

# **Wettability Alteration and Oil Recovery by Water Imbibition at Elevated Temperatures**

SUPRI TR – 114 Report

By  
J. M. Schembre  
G.-Q. Tang  
A. R. Kovscek

December 1998

Prepared for  
U.S. Department of Energy  
Assistant Secretary for Fossil Energy

National Petroleum Technology Office  
P.O. Box 3628  
Tulsa, OK 74101

Prepared by:  
Stanford University  
Stanford, California

# Wettability Alteration and Oil Recovery by Water Imbibition at Elevated Temperatures

J. M. Schembre, G.-Q. Tang, and A. R. Kovscek\*  
Stanford University  
Department of Petroleum Engineering  
Stanford, CA 94305-2220

\*corresponding author, email: kovscek@pangea.stanford.edu, Tel: 650-723-1218

## Abstract

This investigation adopts a new perspective on wettability alteration as a function of temperature. Colloidal (i.e., DLVO) theory and calculations are used to interpret results from laboratory scale displacements. Water imbibition tests were conducted with 9 reservoir cores from a diatomaceous reservoir. Permeability and porosity of cores varied from 0.2 to 0.7 md and 45 to 65%, respectively. The experiments included spontaneous counter current water imbibition followed by forced cocurrent water imbibition to residual oil saturation. The fluids were 34 °API crude oil and synthetic formation brine. All tests were isothermal and temperatures ranged from 45 to 230 °C at pressures sufficient to maintain liquid water. The experimental results show that an increase in temperature results in: (1) a substantial increase in imbibition rate and extent of oil recovery, (2) a slight reduction in residual oil saturation, and (3) a significant shift in the Amott wettability index from intermediate and weakly water wet to strongly water wet. DLVO calculations illustrate detachment of fines from pore surfaces at high temperature. Fines detachment is a mechanism for altering wettability. Release of fines coated with oil exposes clean water-wet pore surfaces. Further calculations indicate the water-oil contact angle decreases as temperature increases indicating a systematic increase in water wettability consistent with experimental measurements of the Amott index.

*Key words:* wettability alteration, water imbibition, temperature, DLVO theory

## 1. Introduction

Steam injection, has been applied successfully to low permeability, hydraulically fractured oil reservoirs containing both relatively light and heavy crude oil (Kumar and Beatty, 1995; Kovscek et al., 1996A&B; Murer et al., 2000). Wettability of the reservoir rock is a key factor in thermal displacement efficiency (Hoffman and Kovscek 2004). Some crude oil/brine/rock systems are noted to shift toward water wetness as a result of heating (Tang and Morrow, 1997; Tang and Kovscek, 2004). The mechanisms of wettability alteration at high temperature, however, remain in question.

Literature review shows different viewpoints on wettability alteration as a function of temperature. Some studies show a decrease in residual oil saturation by water injection with an increase in temperature systematically for both consolidated and unconsolidated systems (Edmondson, 1965, Poston, et al, 1970, Maini and Batycky, 1985). Tang and Morrow (1997) demonstrated for Berea sandstone that an increase in temperature always resulted in increased water-wetness and increased oil recovery by

either spontaneous water imbibition or waterflooding. Similar behavior was also observed for North Sea carbonate rocks (Dangerfield and Brown, 1985). A significant feature is that the Amott index (Amott, 1959) increased with temperature systematically. Tang and Kovscek (2004) found that oil saturation remaining after spontaneous water imbibition into field and outcrop diatomite samples decreased as temperature increased from 45 °C to 180°C. They also report that wettability alteration correlates with fines production at high temperature.

Recently, Schembre and Kovscek (2004) performed a theoretical and experimental study of fines detachment from rock surfaces at elevated temperature. They show that fines detachment in sandstone occurs repeatably at a given temperature for a particular brine salinity and pH. A scenario for wettability shift toward water wetness was proposed whereby the detachment of oil-wet fines from pore walls exposes the clean water-wet pore surfaces underlying fines, Fig.1. The fraction of water wet surface thereby increases.

Al-Hadhrami and Blunt (2001) propose a different model to explain wettability alteration induced by high temperature. They believe direct desorption of asphaltene macromolecules from rock surfaces is responsible for wettability alteration at high temperature. They assume a critical temperature for spontaneous asphaltene desorption from rock surfaces. As a result, the rock surfaces revert to a water-wetness. Similar opinions were expressed by Hjelmeland and Larrondo (1986). This mechanism lacks experimental proof. Furthermore, it is counter to laboratory experience that suggests asphaltene adsorb irreversibly and stably (Clementz, 1982). Strong organic-phase solvents, such as hot pyridine, are generally needed to dissolve asphaltene adsorbed on solids (Yan et al.,1997).

This paper proceeds by describing the experimental apparatus and procedures employed to measure water imbibition rate, ultimate oil recovery, endpoint relative permeability, and wettability of crude oil/brine/field diatomite rocks as a function of temperature. DLVO theory (Derjaguin, Landau, Verwey, and Overbeek, 1987) is developed for calculations of fines stability and the wettability of silica surfaces. Fines production is shown to be a mechanism of wettability alteration towards water-wetness.

## **2. Experimental**

Nine core plugs were sampled from a single well drilled in a diatomite reservoir. The core plugs have a diameter of 2.54 cm and lengths ranging from 4 to 6.6 cm. The measured permeability ranges from 0.2 to 0.7 md and the porosity is from 49 to 65%. The core samples were fully saturated with reservoir brines as received. This fluid was removed from the pore spaces by air displacement followed by placing the core in a vacuum oven at 45°C. Only core #9 was cleaned using toluene before use. Cores were cleaned after tests and any change in porosity and permeability induced by high temperature was measured. Table 1 summarizes core data.

Crude oil from the same diatomite reservoir was used as the oil phase. The oil viscosity is about 5-6 cp at 45°C. The API gravity is 34°. A synthetic reservoir brine with a total salinity of 14454 mg/L and pH of 8.0 was used as the water phase. Table 2 lists the brine composition.

### *2.1. Apparatus*

Fig.2 presents a schematic of the experimental apparatus. A specially designed aluminum coreholder was used. This coreholder is suitable for high temperature, high pressure, and X-ray computed tomography (CT) scanning. The core plug was first coated using high temperature silicone gel, then wrapped with FTP heat shrink tubing. It was then placed inside of the aluminum holder and a confining pressure of 300 psi applied. This coreholder was placed in the chamber of the CT scanner (Shimadzu SCT-4500 T). The outlet of the core was closed after completion of the oil saturation process. A pump circulates water across the inlet face of the core. At high temperature, a back-pressure regulator was used to keep the pore pressure above water saturation pressure. The produced fluids were separated using an oil and water separator. The produced oil volume was recorded versus time for calculating oil production.

Water saturation along the core was monitored by CT-scanning various cross-sections. The voxel dimensions of the scan were 0.15 mm by 0.15 mm by 5 mm. The tube current was 130 mA, the energy level was 130 KeV, and the exposure time was 4.5 s per slice. A total of 12 to 14 slices were collected from inlet to outlet.

### *2.2. Experimental procedure*

A single core was subjected to recovery tests at constant temperatures of 45, 120, 180 and 230°C, respectively. Spontaneous counter-current imbibition of water occurs until oil production ceases. The oil saturation within the core at the end of spontaneous imbibition was referred to as the remaining oil saturation. Each core is then subjected to forced, co-current water imbibition to displace oil to its residual saturation. Specific test steps include:

- a. Saturate the core with 100% synthetic formation brine and measure the permeability and porosity at room temperature. Thereafter, heat the coreholder up to 45°C. During the heating process, the inlet of the coreholder is open to the high-pressure syringe pump operating in constant pressure mode. This avoids pressure build-up due to thermal expansion of rock and fluids.
- b. Flood the core in with oil in a cocurrent fashion to establish initial water saturation. When no further water production was detected, oil relative permeability at initial water saturation was measured.
- c. Conduct a spontaneous water imbibition (counter-current) test until no oil production was observed. Water is pumped across the face of the core at a rate of 0.5 cm<sup>3</sup>/min
- d. CT-scan the core periodically to measure water saturation profiles along the core.
- e. Conduct forced water imbibition (co-current) until no oil production was observed.
- f. Measure water relative permeability at residual oil saturation.
- g. Heat the core to a higher test temperature (120, 180, or 230°C).
- h. Repeat steps a-f.

Additionally, produced water is collected and filtered to perform SEM analysis of produced fines.

### *2.3. CT-image processing*

With the measured, raw CT data, porosity and water saturation as a function of time are obtained. The voxel-by-voxel values of porosity are (Akin and Kavscek, 2003, Wthjack, E. M., 1988) as

$$\phi = \frac{CT_{wr} - CT_{ar}}{CT_w - CT_a} \quad (1)$$

where  $CT$  represents CT number (Hounsfields). The subscripts  $wr$  and  $ar$  signify oil-saturated rock and air saturated rock, respectively; whereas  $w$  and  $a$  represent the water and air bulk fluid phases. Mean core porosity is obtained by averaging porosity for each cross section and then averaging the cross sections. The voxel-by-voxel water saturation,  $S_w$ , is obtained as (Akin and Kavscek, 2003, Zhou et al, 2002).

$$S_w = \frac{CT_{owr} - CT_{or}}{\phi(CT_w - CT_o)} \quad (2)$$

where  $\phi$  is the independently measured porosity from Eq. (1) and the subscript  $owr$  refers to rock containing oil and water.

### 3. Experimental results

Fig.3 presents oil recovery by both spontaneous and forced water imbibition for core #5 at temperatures of 45, 120, 180, and 230°C. Solid lines are oil recovery by spontaneous water imbibition and dashed lines are oil recovery by forced water imbibition. For the forced water imbibition, the pressure drop was about 1.23 atm/cm. The initial water saturation for core #5 ranges from 39.4% to 42.8% at various temperatures. The temperature has a significant effect on spontaneous water imbibition. As the temperature increased from 45°C to 230 °C, the oil recovery by spontaneous water imbibition increased from about 12% OOIP (original oil in place) to about 43% OOIP. Additionally, the oil recovery rate increased systematically with temperature. For forced water imbibition, the oil recovery also increased with temperature, but to a lesser degree.

Similar effect of temperature on water imbibition rate and oil recovery was observed for the other cores. Figs.4a-4d summarizes the test data for spontaneous water imbibition of all cores at each temperature. Fig.4a shows the oil recovery by spontaneous water imbibition at 45°C. The core number listed in the legend corresponds to the order of test. The rate and extent of oil recovery by spontaneous water imbibition varies from the core to core, indicating that wettability of cores is not uniform with depth. The imbibition rate for core #9 and core #7 is obviously slower. This phenomenon may be related to smaller pore size and lesser water-wetness (see Table 1). The oil recovery by spontaneous water imbibition at 45 °C ranges from 10.5% to 23.5% OOIP; the average oil recovery is about 18% OOIP. Fig.4b presents the oil recovery by spontaneous water imbibition at 120°C. The imbibition rate also varies from core to core. Cores #7 and #9 still give the lowest imbibition rate and less oil recovery. Cores #1 and #2 give the highest imbibition rate and greatest oil recovery. The oil recovery by spontaneous water imbibition at 120°C ranges from 25-36 % OOIP with an average of 27% OOIP. Fig.4c presents the spontaneous water imbibition data at 180°C. It shows that both imbibition rate and recovery are improved compared to results obtained at 120°C. Cores #9 and #7 still give the smallest water imbibition rate, but the final oil recovery is improved significantly and is comparable to other cores. This indicates that the wettability of these two cores has shifted. The oil recovery ranges from 35 to 45 % OOIP with an average of 39.6% (OOIP) 180°C. Fig.4d gives the spontaneous water imbibition data for only 7

cores at 230°C because the high-temperature sleeve failed during tests. A significant feature of Fig. 4d is that recovery curves all nearly collapse. This reveals the wettability for all test cores (except for core #9 and #6) is similar at 230°C. Apparently, strong water-wetness has developed for all cores at 230°C as evidenced by rapid imbibition rate and increased oil recovery. The recovery at 230°C ranges from 40-48% OOIP with an average of 43.7 % OOIP.

Fig.5 presents the final water saturation profiles after spontaneous water imbibition as measured by X-ray CT at each test temperature for core #2 (1443.7 ft). The initial water saturation curve (solid diamond) was measured at 45°C. The initial water saturation at different temperatures varies little and the data measured at 45°C are representative of all tests. A water saturation gradient exists along the core as a result of countercurrent imbibition. The water saturation is greater at the open end of the core and lower at the outlet. At 45°C, the final water saturation near the inlet ranges from 0.63 to 0.68 PV. The water saturation near the closed end ranges from 0.39 to 0.44 PV. A gradient in the final water saturation profiles was also measured at higher temperatures, but the gradient gradually decreases with temperature. The change in the water saturation profile as temperature rises from 180 to 230°C is quite small implying little affect from further temperature increase. Similar behavior was obtained for all other cores and is not shown for brevity.

### 3.1. Remaining and residual oil saturation

Figs.6a and 6b present the oil saturation remaining after spontaneous imbibition and the residual oil saturation, respectively, versus depth at the four different test temperatures. For the core from a depth of 1574.3 ft (core #9), Fig 6a shows that the remaining oil saturation is very high (0.88 PV) at 45°C. This test was initiated at zero initial water saturation. Vinsud et al (1999) showed that when initial water saturation is less than some critical saturation, water imbibition efficiency increases with initial water saturation. With the exception of core #9, the average remaining oil saturation is about 0.5 PV at 45°C; it varies between 0.45 to 0.54 PV. As the temperature increased from 45 to 230°C, the remaining oil saturation after spontaneous water imbibition decreased to 0.29 PV (average) and varied from a low of 0.28 to a high of 0.43 PV.

Fig.6b shows the residual oil saturation measured after forced water imbibition. Compared to remaining oil saturation following spontaneous imbibition, the variation in residual oil saturation for a particular core is much less. The effect of temperature on residual oil saturation is small and not systematic. Temperature increase does not always reduce the residual oil saturation (see cores #7, #8, #9, #1). The average residual oil saturation for all cores is 0.26 PV at 45°C, 0.28 PV at 120 °C, 0.23 PV at 180 °C, and 0.22 PV at 230 °C. Overall, the residual oil saturation following forced water imbibition varied little as a function of temperature.

### 3.2. End point relative permeability

The end point relative permeabilities ( $k_{ro}$  at  $S_{wi}$  and  $k_{rw}$  at  $S_{or}$ ) were measured for each core. Note the initial water saturation,  $S_{wi}$ , is defined as the water saturation where no further water production is observed by oil displacement. Residual oil saturation,  $S_{or}$ , is defined as the oil saturation where no further oil production was observed by water

displacement. Thus, the end point oil or water relative permeability was measured by assuming the other phase is not mobile at  $S_{wi}$  or  $S_{or}$ .

Fig.7a shows the measured end point oil relative permeability at  $S_{wi}$  versus temperature for all cores. The data show that the measured end point oil relative permeability is quite scattered and varies among cores at the same temperature. This is caused by variation of initial water saturation and wettability status from core to core. On average, the end point oil relative permeability increases as temperature increases from 45 to 120°C; it then gradually decreases with temperature. The reduction of end point oil relative permeability is only from about 0.25 to 0.2. Fig.7b displays the measured end point water relative permeability versus temperature for all cores. Again the data are varied because the final water saturation varies among cores.

Fig.8 shows the measured end point relative permeability versus water saturation for all cores at four different temperatures. The symbols are the measured data and the solid lines are data fit to a Corey-type relative permeability function. The best fit to the data is

$$\begin{aligned} k_{rw} &= 0.23 S_{wn}^{4.0} \\ k_{ro} &= 0.80 (1 - S_{wn})^{4.0} \\ S_{wn} &= (S_w - S_{wi}) / (1 - S_{or} - S_{wi}) \end{aligned} \quad (3)$$

A best fit to measured end point relative permeability at each test temperature was made. The relative permeability for the test cores displays more sensitivity to water saturation than it does temperature.

#### 4. Wettability alteration

In this section, the test data are interpreted with respect to the Amott wettability index ( $AI_w$ ) and analysis of produced fines is presented.

##### 4.1. Amott index to water

Fig.9a shows the measured Amott Index to water,  $AI_w$ , at reservoir temperature (solid square) and initial clay content (open triangle) versus depth of the core. The Amott index is the fraction of water that imbibes spontaneously upon the total water imbibed to the end of forced imbibition. Note that Amott Index to water at reservoir temperature represents the original wettability of the core. Apparently, core with high clay content has intermediate to mixed wettability as gauged by the Amott index to water, thereby indicating that clay content of the core is an important factor in wettability status. This result is in agreement with Tang and Morrow (1999). They found that removing clays from Berea sandstone by firing and/or acidizing the core resulted in an increase of water wetness. Fig.9b demonstrates the effect of temperature on  $AI_w$ . Our measurement shows that increase in temperature results in an increased  $AI_w$  for all cores. The average  $AI_w$  is 0.35 for 45°C, 0.56 for 120°C, 0.65 for 80°C, and 0.72 for 230°C. The change between 180 to 230°C is small suggesting the temperature effect reaches its maximum beyond 180°C. This result is in agreement with the measure fines production presented next.

##### 4.3. Fines production

Fines production at elevated temperatures has been observed from our previous imbibition tests with different cores (Tang and Kovscek, 2004; Schembre and Kovscek, 2004). The produced fines are yellow to brown and have a long settling time in water.

Particles adhere to laboratory glassware and a strong solvent, such as toluene, is needed for cleaning. The produced fines are oil-wet. Fig.10 shows the fines pictures taken from core #3 at different temperatures. At 45°C, no fines production was observed. As the temperature increased to 120°C, 180°C, and 230°C, fines production was observed. Table 3 lists the fines production data for cores #3 and #6. The initial clay content for these cores was 17.8% and 36%, respectively.

Firstly, more fines production from core #6 than core #3 was observed, indicating the intensity of fines production increases with clay content of the core. Secondly, fines production begins at temperature of 120°C and continues at 180 and 230°C. Thirdly, the particle size ranges from 0.1 to 0.3  $\mu$ . Some fines may be less than 0.1  $\mu$ , but the amount is negligible. After the fines were filtered, the water became clear. Similar phenomenon was observed for other cores (Schembre and Kovscek, 2004).

Fig.11 presents the SEM analysis of fines at both 120 and 180°C. The main elements as measured by elemental dispersive X-ray spectroscopy (EDS) are Al, C, Fe, O, Si, plus minor Ca, Cl, Na. The major compounds are silica, clay, iron oxide, salt, hydrocarbons. The hydrocarbons originate from oil adhering to fines. In addition, the particles are diatom fragments, feldspars, quartz, and mica. Clays, such as kaolinite, were prevalent at 120 and 180 °C. It is noted, however, that relatively more salt and iron oxide were found at 180°C, implying that a significant amount of clay detached from pore surfaces at 120°C. Note that lesser fines production at higher temperature does not mean that an increase in temperature decreases fines production. Recall, the experiments use the same core at successively greater temperatures. Fines production from one temperature to the next greater adds to the cumulative fines production.

## 5. DLVO theory

Forces acting between a charged colloidal particle and a surface in an electrolyte solution are either attractive ( $F_A$ ) or repulsive ( $F_R$ ). In principle, the stability of colloidal systems is explained by the balance of these two interactions. The net interaction is either repulsive or attractive. This idea is referred to as DLVO theory (Derjaguin et al, 1987).

In DLVO theory it is assumed that colloidal particles are very large as compared to electrolyte ions. This makes it possible to express the interaction forces between a particle and a surface,  $F_T$ , as a function of their mutual separation,  $h$ .

$$F_T(h) = F_A(h) + F_R(h) \quad (4)$$

Mathematical expression for these forces depend on the geometry considered, as discussed shortly. The main objective of this section is to develop a systematic understanding of the role that temperature plays on surface forces and extend the general approach to reservoir wettability. Given the different geometries involved for fines detachment and thin film stability, each is treated separately.

### 5.1 Fines stability

The balance between the forces affecting the attachment of a particle to a rock surface determines the stability or detachment of fines/clay particles. The analysis assumes that aqueous fluid is in contact with the pore surface and fines, as indicated in Fig. 1. Two geometries representative of the fine/particle – pore surface interaction are employed: (a) sphere-plate system (Fig.12a) and, (b) cylinder-plate system (Fig.12b).

### 5.1.1. Sphere-plate systems

The interaction between a particle and a pore surface is described by an extension of Eq (4):

$$V_i(h) = V_{LVA}(h) + V_{DLR}(h) + V_{BR}(h) \quad (5)$$

where V is the interaction potential and subscripts represent the London Van Der Waals (LVA) attraction, the double layer repulsion (DLR), and the Born repulsion (BR). It is assumed that short-range forces such as hydrated layer and structural forces are negligible.

The Van der Waals dispersive forces are attractive. They play an important role with respect to intergranular and wetting behavior. The ratio of the distance of separation, h, to the particle radius,  $r_p$ , is much less than unity and, accordingly, the effects of retardation of electromagnetic waves are ignored. Thus, the London Van-der Waals potential for sphere-plate system is estimated numerically as (Hamaker, 1937):

$$V_{LVA}(h) = -\frac{A}{6} \left[ \frac{2(H+1)}{H(H+2)} + \ln\left(\frac{H}{H+2}\right) \right] \quad (6)$$

where H (= h /  $r_p$ ) is the ratio of the distance of separation to particle radius and A is the Hamaker constant.

Hamaker's pair-wise summation procedure is used to calculate the combined Hamaker constant of two macroscopic identical and different particles interacting in a third medium. For two identical materials (e.g. silica-silica systems) in water, the Hamaker combining rule is

$$\begin{aligned} A_{sws} &= A_s + A_w - 2A_s A_w \\ A_{sws} &= \left( \sqrt{A_s} - \sqrt{A_w} \right)^2 \end{aligned} \quad (7)$$

in which  $A_s$  and  $A_w$  refer to the silica and water Hamaker constants respectively, in vacuo. The value of the Hamaker constant estimated for silica-water-silica system is 0.36E-20 J. correspondingly, for different materials (e.g. silica-kaolinite) in water, the Hamaker combining rule is described by:

$$\begin{aligned} A_{swk} &= A_{sk} + A_w + A_{sw} - A_{kw} \\ A_{swk} &= \left( \sqrt{A_s} - \sqrt{A_w} \right) \left( \sqrt{A_k} - \sqrt{A_w} \right) \end{aligned} \quad (8)$$

The value of the Hamaker constant estimated for the system silica-water-kaolinite is 2.26E-20 J. The Hamaker constant for ceramic systems is reported to change only 3% over the range 27 – 200 °C (French, 2000). This variation is small considering changes in the other terms in Eq. 5. Temperature sensitivity of A is consequently neglected.

The double layer repulsion term,  $V_{DLR}(h)$ , is calculated assuming constant surface charge:

$$V_{DLR}(h) = \frac{\varepsilon r_p}{4} \left( \Phi_{01}^2 + \Phi_{02}^2 \right) \left[ \frac{2 \Phi_{01} \Phi_{02}}{\Phi_{01}^2 + \Phi_{02}^2} \ln\left(\frac{1 + \exp(-\kappa h)}{1 - \exp(-\kappa h)}\right) - \ln(1 - \exp(-2\kappa h)) \right] \quad (9)$$

where  $\varepsilon$  is the dielectric constant of the medium and  $\Phi_{0i}$  is the surface potential of the wall (i=1) and particle (i=2). The Debye-Huckel reciprocal,  $\kappa$ , length is

$$\kappa = \sqrt{\frac{2e^2 n_b}{\epsilon k T}} \quad (10)$$

where  $n_b$  is the total ion density in bulk.

The potential of each surface,  $\Phi_{oi}$ , is taken to be  $\zeta_i$ , the electrical potential at the boundary between the Stern layer and the diffuse layer. In turn, the zeta potential is approximated by the Nernst equation:

$$\zeta_i = \Phi_{oi} = -2.3 \left( \frac{kT}{e} \right) (pH - pH_{oi}) \quad (11)$$

where  $pH_{oi}$  is the isoelectric point of surface  $i$ .

The Born repulsion,  $V_{BR}(h)$ , measures the short-range molecular interaction resulting from the overlap of electron clouds. It is suggested to follow the relationship (Kia, 1987)

$$V_{BR} = \frac{A\delta^6}{7560} \left[ \frac{8r_p + h}{(2r_p + h)^7} + \frac{6r_p - h}{h^7} \right] \quad (12)$$

where  $\delta$  is the collision diameter. It is assigned a value of approximately 5 Å (Khilar and Fogler, 1987).

### 5.1.2. Cylinder-plate systems

The balance of attractive and repulsive forces is provided by Eq.(5). The expression for the non-retarded van Der Waals forces (Mahmood et al, 2001, Isrealachivili, 1991) is

$$F_{LVA} = -\frac{A}{8\sqrt{2}} \left( \frac{l}{r_p^2} \right) \left( \frac{r_p}{h} \right)^{\frac{5}{2}} \quad (13)$$

where  $l$  is the length of the cylinder. The double layer repulsion term,  $F_{DLR}(h)$ , is calculated using the linear superposition approximation (LSA) (Mahmood et al, 2001).

$$F_{DLR} = 32\sqrt{2}\epsilon\kappa\sqrt{\pi\kappa r_p} \left( \frac{kT}{ez} \right)^2 \tanh\left( \frac{ez\zeta_1}{4kT} \right) \tanh\left( \frac{ez\zeta_2}{4kT} \right) \exp(-\kappa h) \quad (14)$$

We refer to the detachment temperature of a fine as the temperature where the resulting potential,  $V_t$ , switches as from attractive to repulsive for a given salinity and pH. Natural diatomite is composed of mostly amorphous silica. Therefore, the flat surface is taken as silica. With respect to the fines material, SEM images showed both silica and kaolinite in the effluent. We present the detachment temperature for sphere-plate and cylinder-plate interactions for various conditions in silica-kaolinite and silica-silica systems.

### 5.1.3. Calculations

Published data for  $\zeta$  potential is relatively sparse with respect to the range of pH, T, and salinity relevant to steam condensate. Consequently, the prefactor in Eq.(8) was regressed so that predicted values of  $\zeta$  agreed with published values for kaolinite and silica. The expression was then used for interpolation and extrapolation among the measured values. Fig.13 shows measured and computed values of  $\zeta$  versus pH at 25 °C for (a) silica (Berli, 2003) and (b) kaolinite (Vane and Zhang, 1997). The zeta potential as

a function of temperature is obtained by fitting values of zeta potential reported in the literature for different temperatures, materials and fluid conditions (Ramachandran and Somasundaran, 1986, Somasundaran and Kulkarni, 1973, Pagneoux et al, 1998, Dai and Chung, 1995, Revil, et al, 1999). The resulting correlation is

$$\zeta(T) = 0.01712((T - T_0) + 1) + \zeta(T_0) \quad (15)$$

where temperature is in K,  $T_0$  is the measurement temperature for  $\zeta(T_0)$ , and  $\zeta(T)$  is the correlated value at the same pH and salinity as  $\zeta(T_0)$ . Fig.14 gives a cross plot of the reference values versus calculated zeta potential. According to the literature reviewed, all materials follow a similar behavior with increasing temperature: the zeta potential becomes more negative as the temperature increases indicating stronger repulsive forces.

#### 5.1.4. Results

In a static fluid environment, fines are released from the solid when the interaction potential is zero. Repeated calculation of the total potential for combinations of temperature, fluid pH, and salt concentration identifies the conditions where sphere /cylinder (fines) and plate (grain surface) interactions are no longer attractive. Fig.15 shows contour maps of detachment temperatures parameterized by pH and salinity for (a) silica-silica (b) kaolinite-silica systems using the sphere-plate model. Similar calculations for cylinder-plate model are shown in Fig.16. The salt concentrations (salinity) ranges between 0.001 and 0.5 M (100 and 14,000 ppm) and pH values from 5 to 14. For low salinity and high pH, the resulting potential at room temperature is mostly repulsive indicating fines release. These results show the same trend as reported by Schembre and Kovscek (2004).

The cylinder-plate model is more sensitive to the effect of temperature than the sphere-plate model for both, silica-silica and silica-kaolinite, systems. Note that the, silica-silica system is more sensitive to temperature than the silica-kaolinite system. In the experiments, fines were produced at a temperature of 120°C. This detachment temperature agrees with the range obtained for the cylinder-plate system. The detachment temperature for silica-silica is around 80°C, indicating that silica particles might have detached at temperatures less than the temperature at which the system was operating.

It is important to notice that the brine used in the experiment contained a small amount of calcium ion that diminishes the zeta potential due to compression of the electrical double layer. This results in a system that is less sensitive to temperature changes.

#### 5.2 Thin wetting film stability

When the thickness of the water phase becomes comparable to the thickness of the interfacial region (overlapping of interfaces) the properties of the bulk water phase no longer exist in the interlayer. An external (i.e., disjoining) pressure is needed to maintain a constant film thickness, and further decreases in film thickness require additional work. The disjoining pressure ( $\Pi$ ) acts normal to the film and it opposes film thinning. Fig 17 compares disjoining pressure isotherms for completely and partially water-wet systems. In the case of zero capillary pressure and a flat surface, the condition of marginal stability is that the interaction potential has a local maximum between the thick, wetting film and the thin film (Hirasaki, 1991), as illustrated in Fig.17.

The role of the water film is absolutely essential. The presence of thick water films between the crude oil and the rock surface prevents asphaltenes within the oil phase from contacting the rock and accordingly thick water films protect against wettability change (Kovscek, et al, 1993). Wettability is related to thin film forces through the contact angle,  $\theta$ , and the disjoining pressure,  $\Pi$ , by (Derjaguin, 1940)

$$\cos\theta - 1 = \frac{1}{\sigma} \left[ \int_{h_x}^{\infty} \Pi(\xi) d\xi + h_x \Pi(h_x) \right] \quad (16)$$

where  $h_x$  is the equilibrium film thickness of interest. Integration over the positive, purely repulsive, thick outer film results in zero contact angle. Equally, non-zero contact angles are possible when Eq. (16) is integrated over the attractive negative portions (Kovscek, et al, 1993).

### 5.2.1. Disjoining pressure calculations

The disjoining pressure acting between the crude oil and solid surface is a composite of London Van der Waals attractive forces,  $F_{LVA}(h)$  and electric double layer force,  $F_{DLR}(h)$ . The hydration force is assumed to be zero in these calculations. The retarded Van der Waals attractive forces between two parallel plates is (Gregory, 1981)

$$F_{LVA}(h) = - \frac{A(15.96 h / \lambda + 2)}{12\pi h^3 (1 + 5.32 h / \lambda)^2} \quad (17)$$

The Hamaker constant for oil/silica in water is approximately  $1E-20$  J (Takamura and Chow, 1983) and the London wavelength assumed is 100 nm (Takamura and Chow, 1983, Buckley et al, 1989). The electric double layer force for interfaces possessing different potentials,  $\zeta_1$  and  $\zeta_2$ , is estimated under the constant potential approximation, described by Gregory (1975)

$$F_{DLR}(h) = n_b kT \left\{ \frac{\Phi_{r1} \Phi_{r2} \cosh(\kappa h) - \Phi_{r1}^2 - \Phi_{r2}^2}{(\sinh(\kappa h))^2} \right\} \quad (18)$$

where  $\Phi_{ri}$  is the reduced potential ( $\Phi_{ri} = e\zeta_i / kT$ ). The zeta potential is approximated by Eq. 11 and, fit to experimental values provided in the literature, with respect to salinity, pH and temperature. The zeta potential values for the oil phase were those obtained for Moutray Oil (Buckley et al, 1989). Moutray oil is a 35.2 API similar to the crude oil used in the experiments. Experimental and calculated zeta potential values for Moutray crude oil are compared in Fig.18 and show good agreement.

### 5.2.2. Results

Fig. 19 shows the disjoining pressure isotherms for silica/water/crude oil system at a pH of 8 and brine salinity of 0.5 M at the four experimental temperatures. As the temperature increases, the maximum in the disjoining pressure isotherm increases. Between 180 and 230 °C the maximum disjoining pressure increases from 182 kPa (1.8 atm) to 689 kPa (6.8 atm). The equilibrium contact angle at 45, 120, 180, and 230 °C as given by Eq 16. is 18.3°, 19.1°, 13.0°, and 0°, respectively. Hence, water film stability increases substantially with temperature in this example.

The impact of the temperature depends on the salinity and pH of the system. Figure 20 plots the maximum in the disjoining pressure as a function of salt concentration and pH. Film stability decreases as salt concentration increases at constant pH. Similarly, film stability increases with increasing pH for low salt concentration. In all cases, an increase in temperature leads to an increase in the maximum of the disjoining pressure, and consequently, an increase in the stability of the water film.

## 6. Conclusions

This work provides experimental and theoretical proof indicating that temperature affects the wettability of diatomite reservoir rock positively. An increase in temperature reduces the oil to water viscosity ratio, so as to yield a less resistant force to water imbibition, and also enhances the water wetness of solid surfaces. As a result, both imbibition rate and the extent of oil recovery by spontaneous imbibition is improved. Nevertheless, the residual oil saturation is little affected by temperature. Based on the experimental observation and theoretical study, a mechanism for wettability shift toward increased water-wetness at elevated temperature is fines detachment from oil coated pore walls. Fines detachment exposes the clean water-wet rock surfaces underlying fines. The clay content of cores correlates with lesser water-wetness and high clay content cores exhibit significant variation rate of imbibition performance as temperature is increased. Finally, temperature increase is predicted to increase the stability of aqueous water films on pore surfaces.

## Acknowledgements

Portions of this work were prepared with the support of the U.S. Department of Energy, under Award No. DE-FC26-00BC15311. However, any opinions, findings, conclusions, or recommendations expressed herein are those of the authors and do not necessarily reflect the views of the DOE. Additional financial support was provided by the Stanford University Petroleum Research Institute (SUPRI-A) Industrial Affiliates.

## References

1. Akin, S. and A. R. Kovscek, "Computerised Tomography in Petroleum Engineering Research," in Applications of Computerized X-ray Tomography in Geology and Related Domains, Jacobs, P., Mees, F., Swennen, R, Van Geet, M. (eds), Special Publication, Geological Society, London, 215, 23-38 (2003).
2. Akin, S., Schembre, S.K., Bhat, S.K., and Kovscek, A.R., "Spontaneous Imbibition Characteristics of Diatomite," JPSE, 25 (2000) 149-165.
3. Al-Hadhrami, H. and Blunt, M., "Thermally Induced Wettability Alteration to Improve Oil Recovery in Fractured Reservoirs," SPEREE (June 2001)., pp.179-186.
4. Amott, E., "Observations Relating to the Wettability of Porous Media," Trans, AIME, (1959)., 216, 156., pp.
5. Berli, C. L. A., M. V. Piaggio, and J. A. Deiber: "Modeling the zeta potential of Silica Capillaries in relation to the background electrolyte composition," Electrophoresis 2003, 24, 1587-1595.
6. Buckley, J. S., Takamura, K., Morrow, N. R.: "Influence of electrical surface charges on the wetting properties of crude oil. Soc. Pet. Eng. 4, 332. (1989)

7. Clementz, D. M., "Alteration of Rock Properties by Adsorption of Petroleum Heavy Ends: Implication for Enhanced Oil Recovery," paper PSE 10683 presented at third SPE/DOE Joint Symposium on Enhanced Oil Recovery of the Society of Petroleum Engineers held in Tulsa, OK, April 4-7, 1982.
8. Dai, Q. and Chung, K. H.: "Bitumen-sand Interaction in Oil in Sand Processing," *Fuel*, Vol 74, No. 12, pp. 1858-1864, 1995.
9. Dangerfield, J.A., and Brown, D.A., "The Ekofisk Field: North Sea Oil and Gas Reservoirs, J. Kleepe et al. (eds), Graharm and Trotman, London (1985), pp.3-22.
10. Derjaguin, B. V., "Tiyra Kapillyarnoy Kondensatsii and Drugix Kapillapnvix Yavlenii Uchetom Rasklinivayushchevo Daystviya Polimolekuyarnox Shidi Plenox," *Zh. Fiz. Khim.*, 14, 137 (1940).
11. Derjaguin, B.V., Churaev, N.V. and Muller, V.M., "Surface Forces," 1987 Consultants Bureau, New York, A division of Plenum Publishing Corporation, 233 Spring Street, New York, NY 10013.
12. Edmondson, T.A.: "Effect of Temperature on Waterflooding," *JCPT.*, (Oct-Dec., 1965), pp. 236-242.
13. French, R. H.: "Origins and Applications of London Dispersion Forces and Hamaker Constants in Ceramics," *J. Am. Ceram. Soc.*, 83 [9] 2117-46 (2000).
14. Gregory, J: "Interaction of Unequal Double Layers at Constant charge," *J. Colloid Interface Sci.* (1975) 51, 44-51.
15. Gregory, J: "Approximate expressions for retarded Van der Waals Interaction," *J. Colloid Interface Sci.* (1981) 83, 138-145.
16. Hamaker, H. C.: "The London-Van der Waals Attraction between Spherical Particles," *Physics*, 4, 1058 (1937).
17. Hirasaki, G. J.: "Wettability: Fundamentals and Surface Forces," SPE 17367. SPE Formation Valuation, June 1991, pp 217-226.
18. Hjelmeland, O.S. and Larrondo, L.E., "Experimental Investigation of the Effects of Temperature, Pressure, and Crude Oil Composition on Interfacial Tension Properties," SPEFE (July 1986), pp.321-328.
19. Hoffman and Kovsky, "Efficiency and Oil Recovery Mechanisms of Steam Injection into Low Permeability, Hydraulically Fractured Reservoirs," *Petroleum Science and Technology*, Vol.22, Nos. 5 & 6, pp. 537-564, 2004.
20. Isrealachivili, J. N., *Intermolecular and Surface Forces*, second Ed., Academic Press, New York, 1991.
21. Kia, S. F.: "Effect of Salt Composition on Clay Release in Berea Sandstone," SPE paper 16524. Proceedings of the SPE International Symposium on Oilfield Chemistry. San Antonio, Texas, February 4-6, 1987.
22. Khilar K.C. and H. S. Fogler: "Colloidal Induced Fine migration in porous media, *Reviews in Chemical Engineering*, n. 4, 1987, pp 41-108.
23. Kovsky, A. R., H. Wong and C. J. Radke: "A pore-Level Scenario for the Development of Mixed Wettability in Oil Reservoirs," *Environmental and Energy Engineering, AIChE Journal*, June 1993, Vol. 39, No. 6. pp 1072-1085.
24. Kovsky, A.R., Johnston, R.M., and Patzek, T.W., "Interpretation of Hydrofracture Geometry During Steam Injection Using Temperature Transients I. Model Formulation and Verification," *In Situ*, 20 (3), 251-288 (1996).

25. Kovscek, A.R., Johnston, R.M., and Patzek, T.W., "Interpretation of Hydrofracture Geometry During Steam Injection Using Temperature Transients I. Model Formulation and Verification," *In Situ*, 20 (3), 289-309 (1996).
26. Kumar, M., and Beatty, F.D., "Cyclic Steaming in Heavy Oil Diatomite," paper SPE 29623 presented Western Regional Meeting, held in Bakersfield, CA, March 8-10, 1995.
27. Mahmood, T., A. Amirtharajah, T. W. Sturm and K. E. Dennett: "A Micromechanics Approach for Attachment and Detachment of asymmetric Colloidal Particles," *Colloids and Surfaces A: Physicochemical and Engineering Aspects* 177 (2001) pp. 99-110.
28. Maini, B.B. and Batycky, J.P., "Effect of Temperature on Heavy-Oil/Water Relative Permeabilities and Vertical Drilled Core Plugs," *JPT* (Aug. 1985), pp.1500-1510.
29. Murer, A.S., McClennen, K.L., Ellison, T.K., Larson, D.C., Timmer, R.S., Thomsen, M.A., and Wolcott, K.D., "Steam Injection Project in Heavy-Oil Diatomite," *SPEREE* 3 (1) Feb., 2000.
30. Pagneoux, C., M. Serantoni, R. Laucournet, T. Chartier, and J. F. Baumard: "Influence of the Temperature on the Stability on Aqueous Alumina Suspension." *J. Am. Ceram. Soc.*, 1998. pp 1935 – 1948.
31. Poston, S.W., Israel, S., Hossain, A.K., Montgomery, III, and Ramey, H.J.Jr., "The Effect of Temperature on Irreducible Water Saturation and Relative Permeability of Unconsolidated Sands," *Soc. Pet.. Eng. J. (June, 1970).*, pp. 170-180.
32. Ramachandran, R. and P. Somasundaran: "Effect of Temperature on the Interfacial Properties of Silicates," *Colloids and Surfaces*, 21 (1986) 355-369.
33. Revil, A., P. A. Pezard and P. W. J. Glover: "Streaming potential in porous Media: 1. Theory of the zeta potential," *Journal of Geophysical Research*. Vol 104. No. B9, pp 20,021-20,031, September 1999.
34. Somasundaran and R. D. Kulkarni: "A New Streaming Potential Apparatus and Study of Temperature Effects using it," *Journal of Colloid and Interface Science*, Vol. 45. No 3, December 1973.
35. Schembre, J.M., and Kovscek, A.R., "Thermally Induced Fines Mobilization: Its Relationship to Wettability and Formation Damage," SPE 86937 presented at the 2004 International Thermal Operations and Heavy-Oil Symposium and Western Regional Meeting, held in Bakersfield, CA, March 16-18, 2004.
36. Takamura, K. and R. S. Chow: "A Mechanism for Initiation of Bitumen displacement from oil sand," *The Journal of Canadian Petroleum Technology*, pp 22-30. (1983).
37. Tang, G. and Kovscek, A.R., "Experimental Study of Heavy Oil Production from Diatomite by Water Imbibition at Elevated Temperatures," SPE paper 75132 presented at the SPE/DOE Thirteenth Symposium on Improved Oil Recovery held in Tulsa, OK., 13-17 April, 2002.
38. Tang, G., and Kovscek, A.R., "An Experimental Investigation of the Effect of Temperature on Recovery of Heavy-Oil from Diatomite," *SPEJ*, to appear June, 2004.
39. Tang, G. and Morrow, N.R., "Salinity, Temperature, Oil Composition, and Oil Recovery by Waterflooding," *SPERE* (Nov., 1997), pp.269.

40. Tang, G. and Morrow, N.R., "Influence of Brine Composition and Fine Particles on Crude Oil/Brine/Rock Interactions and Oil Recovery," J. of Pet. Sci. & Eng., (Dec. 1999), Vol. 24, pp. 99-111.
41. Vane, L. M. and G.M. Zang: "Effect of Aqueous phase properties on clay particle zeta potential and electro-osmotic permeability: Implications for electrokinetic soil remediation processes," Journal of Hazardous Materials 55 (1997) 1-22.
42. Viksund, B.G., Morrow, N.R., Ma, S., Wang, W., and Graue, A., "Initial Water Saturation and Oil Recovery from Chalk and Sandstone by Spontaneous Imbibition," Proceedings of 1998 International Symposium of the Society of Core Analysts," held in Hague, 14-16 Sept., 1998.
43. Yan, J., Plancher, H., and Morrow, N. R., "Wettability Changes Induced by Adsorption of Asphaltenes," paper SPE 37232 presented at the 1997 SPE International Symposium on Oilfield Chemistry held in Houston, TX., 18-21 February 1997.
44. Zhou, D, Jia, L. Kamath, J., and Kovscek, A.R., "An Investigation of Counter-Current Imbibition Processes in Diatomite," Journal of Petroleum Science and Engineering, 33(1-3), (2002), 61-74.

Table 1 Field diatomite core data

Core No.	Depth ft	L cm	d cm	$\phi$ %	k md	Sq(k/ $\phi$ )
5	1430.4	4.4	2.54	54.2	0.324	0.773
2	1443.7	4.7	2.54	59.1	0.391	0.813
4	1445.7	5.0	2.54	53.9	0.236	0.662
7	1504.9	6.4	2.54	52.5	0.227	0.656
8	1542.3	4.7	2.54	49.3	0.195	0.628
9	1574.3	4.8	2.54	46.1	0.171	0.608
1	1586.6	6.1	2.54	58.4	0.653	1.058
3	1592.8	5.5	2.54	65.1	0.534	0.908
6	1613.2	6.1	2.54	64.9	0.293	0.671

Table 2 Brine composition

Ions	mg/L	M
Na <sup>+</sup>	4900	0.00525
K <sup>+</sup>	34	0.00857
Ca <sup>2+</sup>	210	0.213
Mg <sup>2+</sup>	240	0.00087
Cl <sup>-</sup>	8200	0.23098
HCO <sub>3</sub> <sup>2-</sup>	870	0.001426
Total	14454	0.47293
pH	8.0	

Table 3 Fines production data for cores #3 and #6

Core #	T, C	0.3 $\mu$ >d>0.45 $\mu$	0.45 $\mu$ <d<0.1 $\mu$	Total	Color
3	45	0	0	0	N/A
	120	27 mg	28 mg	55 mg	Yellow
	180	17 mg	16 mg	33 mg	Yellow
	230	2 mg	6 mg	8 mg	Yellow
6	45	0	0	0	N/A
	120	44 mg	38 mg	82 mg	Yellow
	180	33 mg	25 mg	58 mg	Yellow
	230	6 mg	9 mg	15 mg	Yellow

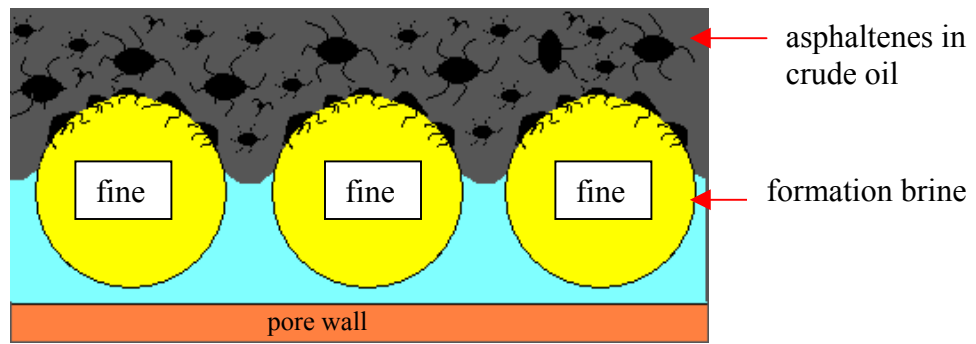


Fig.1 Schematic of fines adhering to pore surfaces.

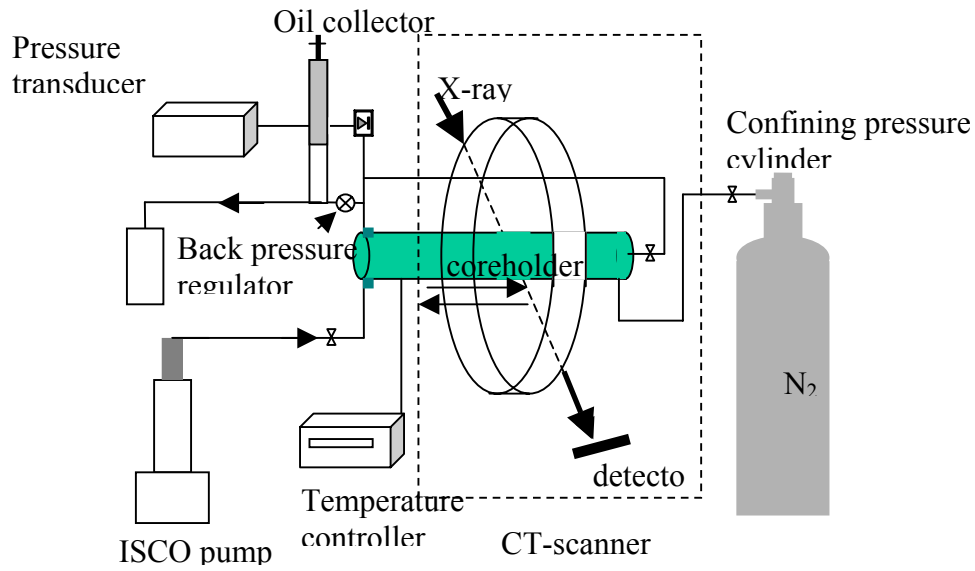


Fig.2 Schematic of the experimental setup

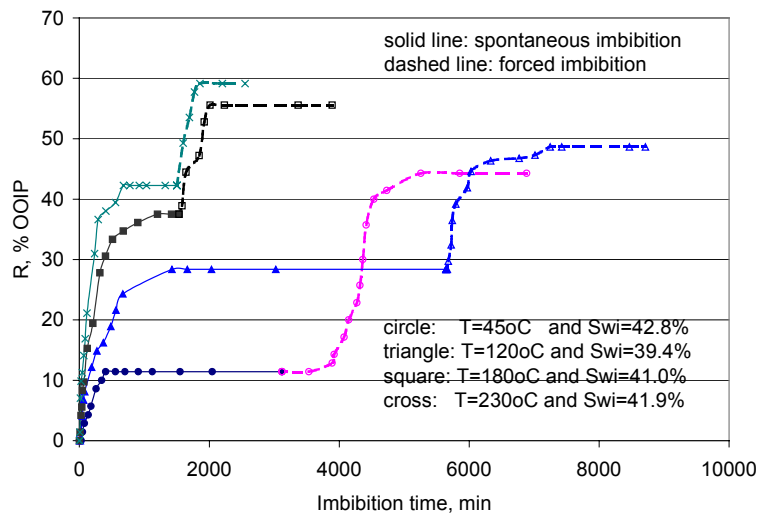


Fig.3 Water imbibition recovery at various temperatures for core #5

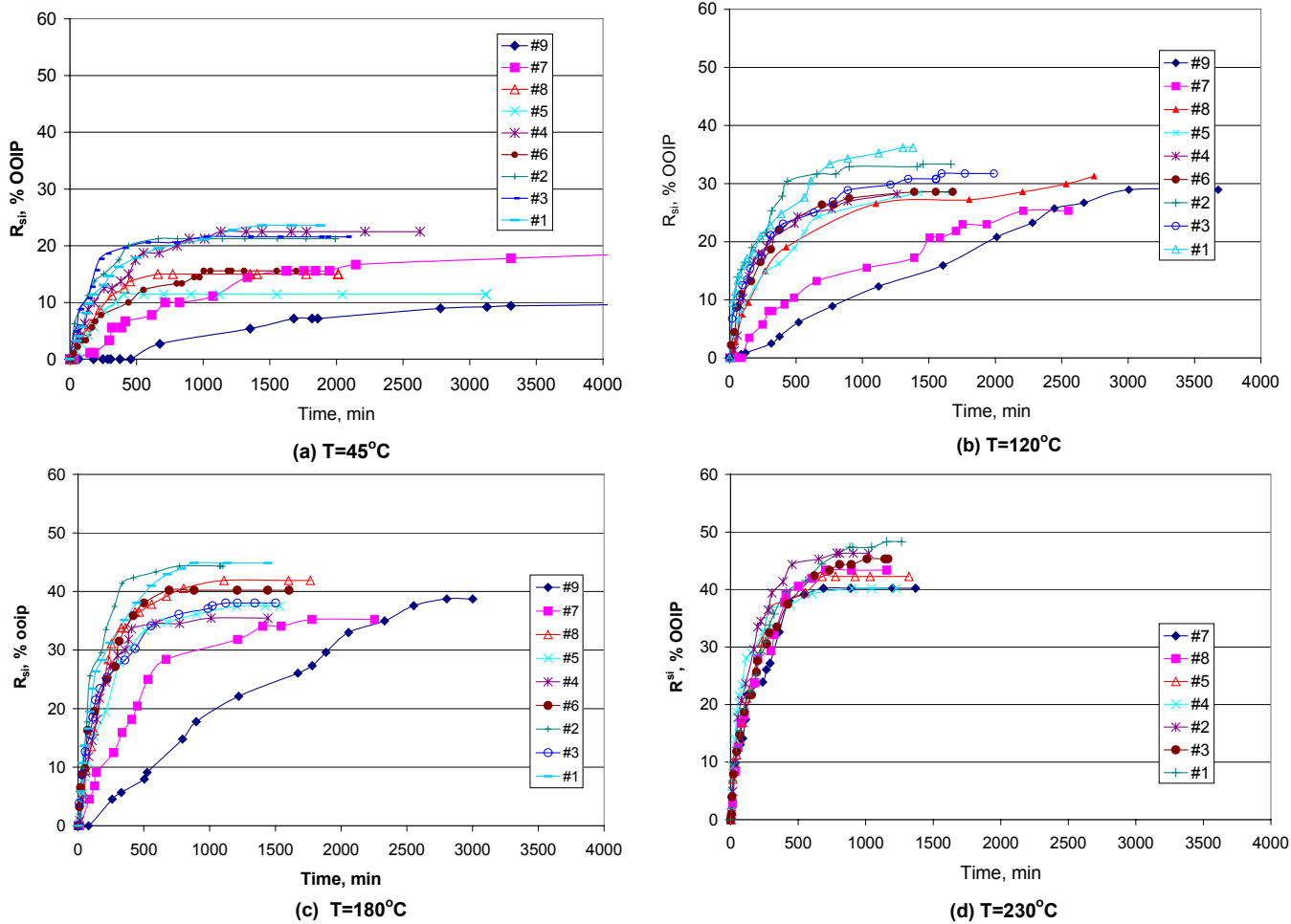


Fig. 4 Oil Recovery by spontaneous water imbibition

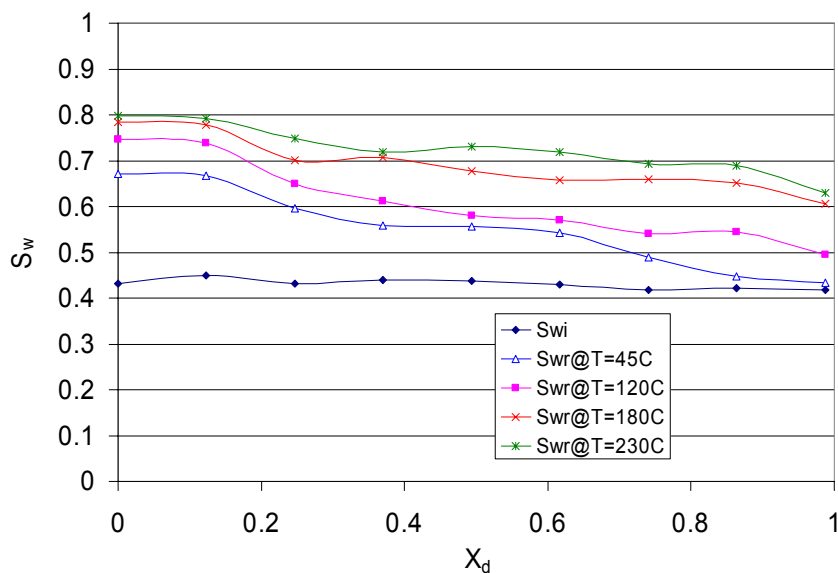


Fig. 5 Water Saturation Profiles after Spontaneous Imbibition: Core #2 (1443.7 ft)

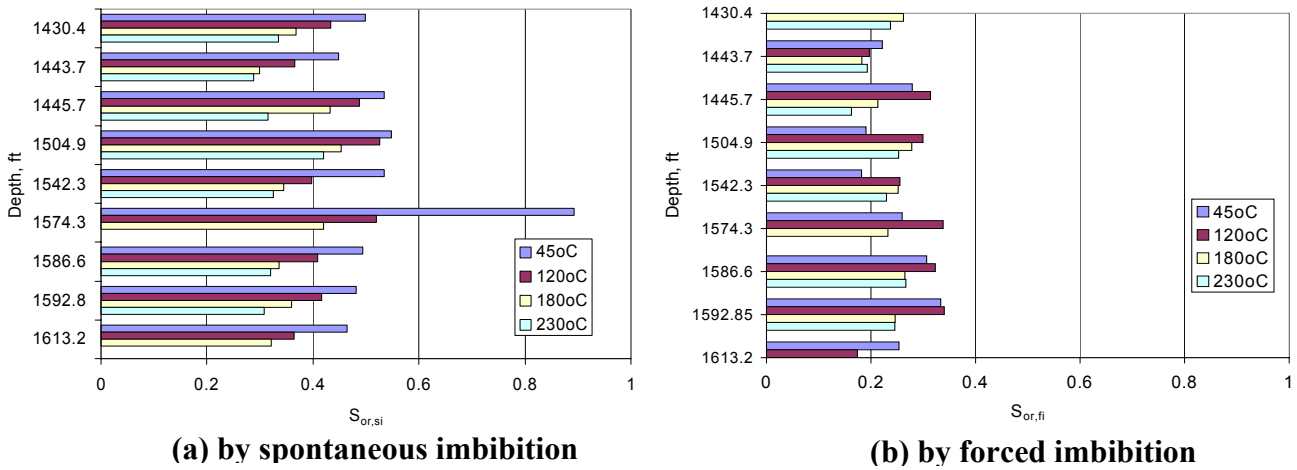


Fig. 6 Residual oil saturation with depth

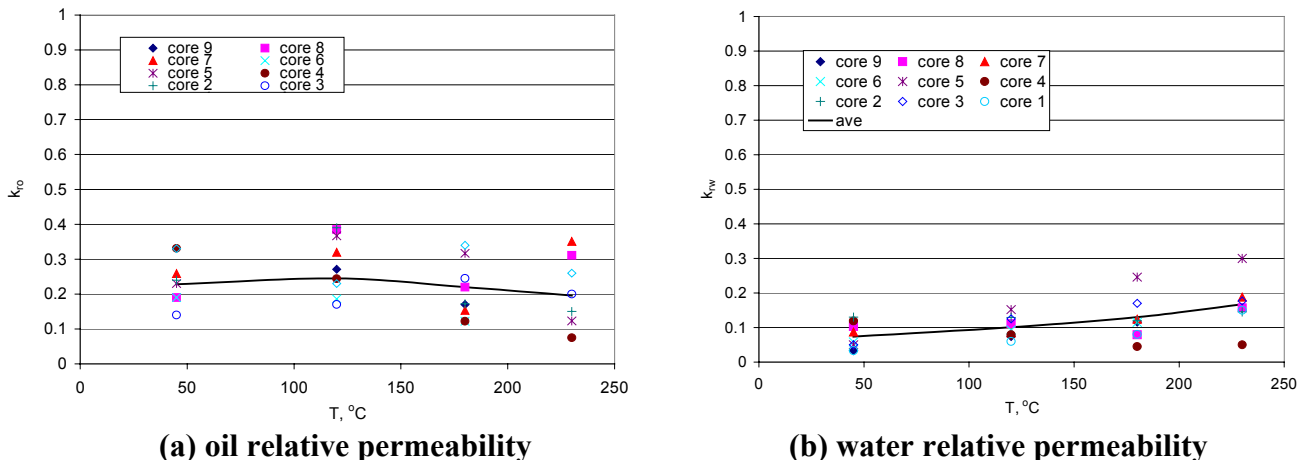


Fig. 7 Effect of temperature on end point relative permeabilities

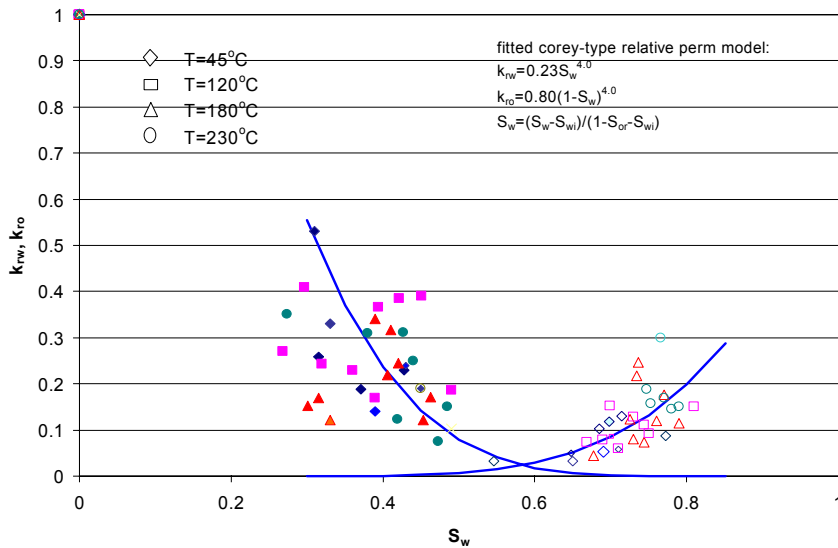


Fig. 8 End point relative permeability versus water saturation

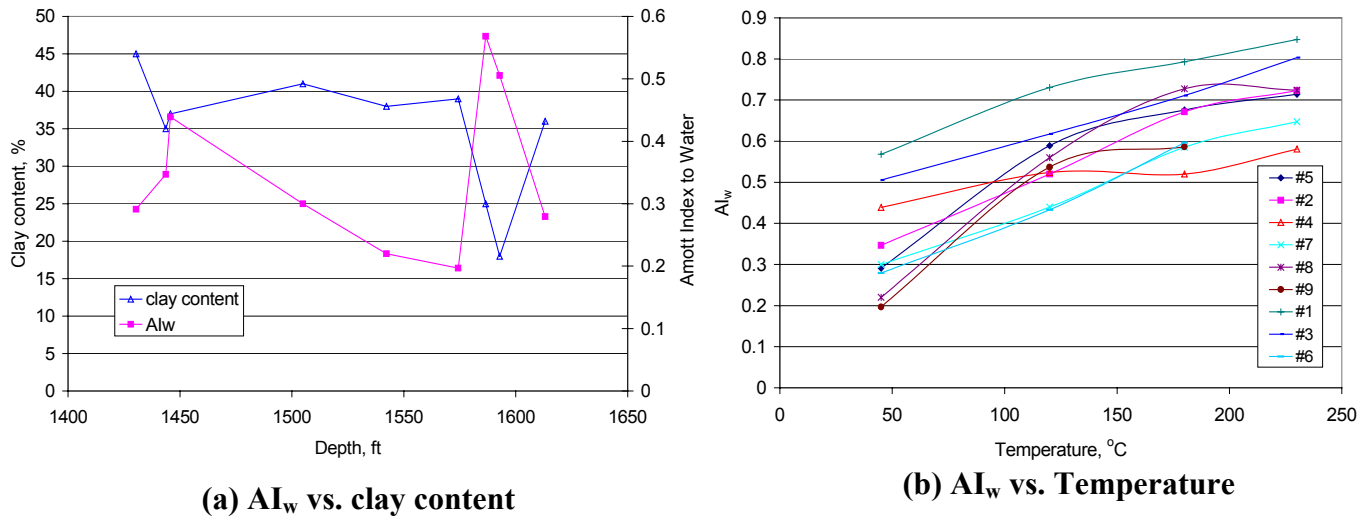
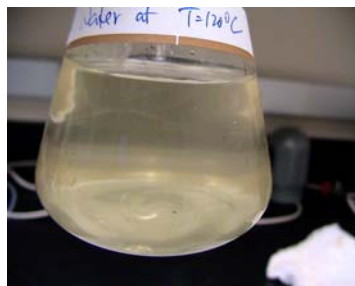


Fig. 9 Amott index to water



T=45°C



T=120°C



T=180°C

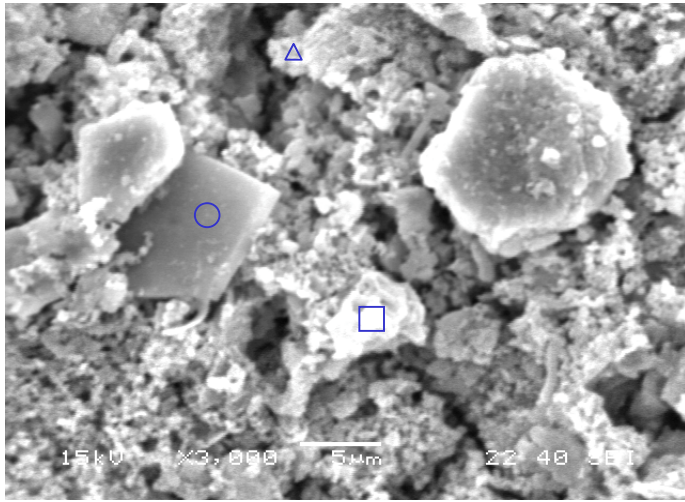


T=230°C

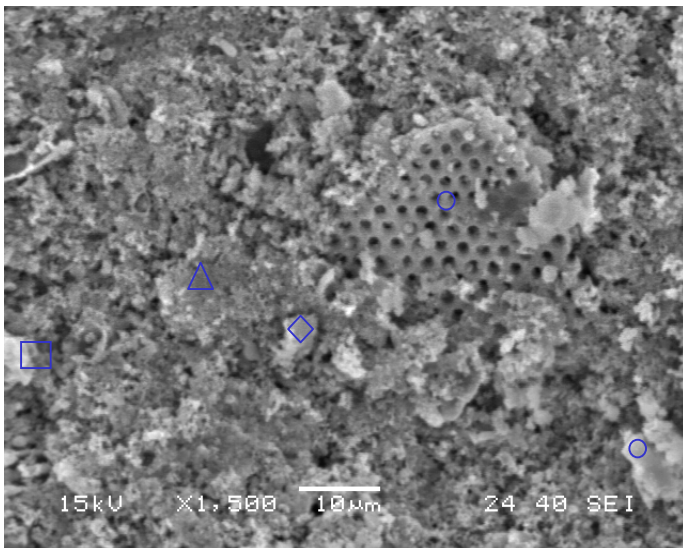
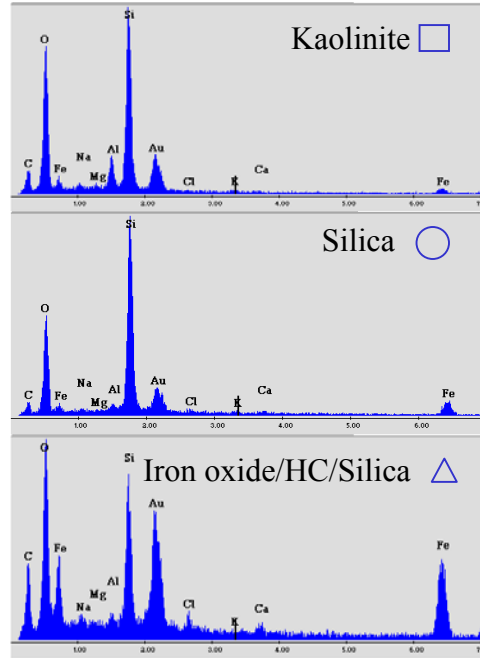


Fines adsorbed on glass surfaces

Fig. 10 Fines Production at Various Temperatures



(a) fines at T=120 °C



(b) fines at T=180 °C

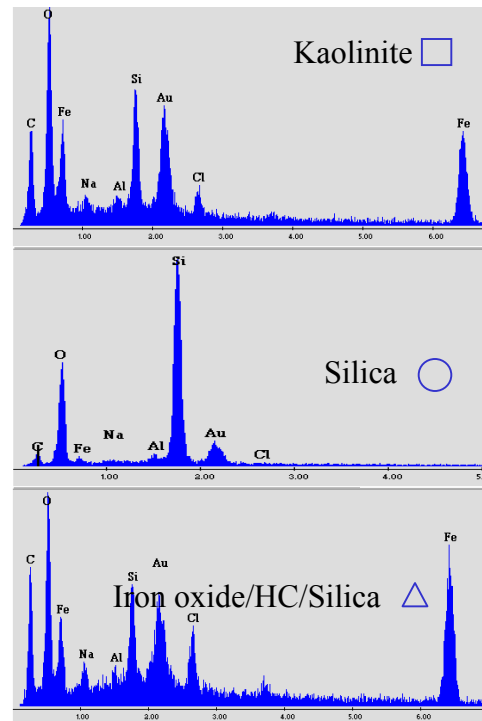


Fig. 11 SEM analysis of produced fines  
(EOS spectra of the various regions marked in the SEM view are given to the right)

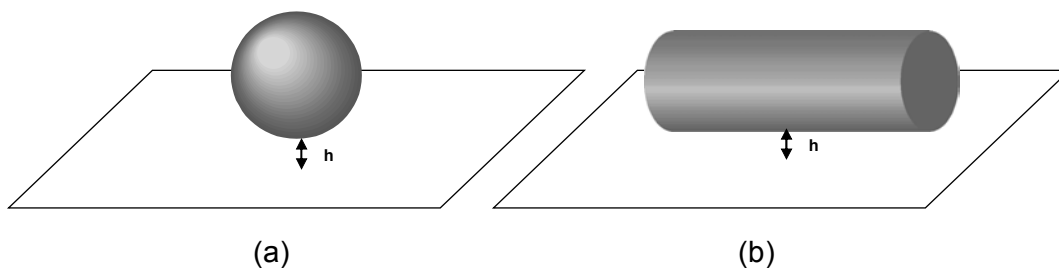


Fig.12 Geometry considered for fines migration calculations: (a) flat plate-sphere and (b) flat plate-cylinder

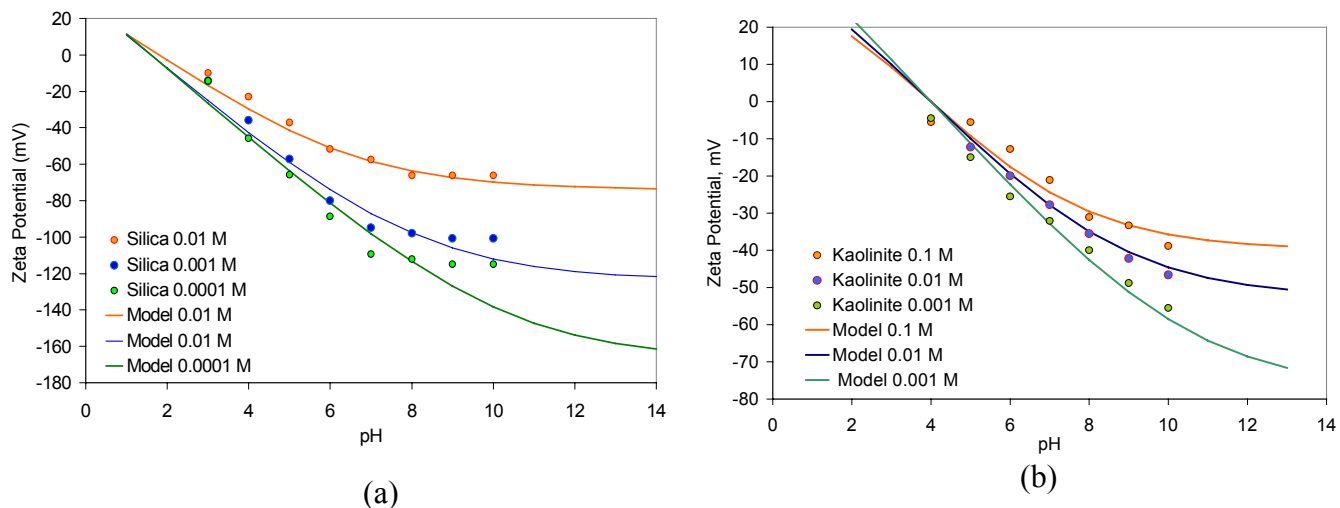


Fig.13 Zeta Potential used in calculations: (a) Silica: Symbols represent experimental values (Berli et al, 2003) and solid lines represent model (b) Kaolinite: Symbols represent experimental values (Vane and Zang, 1997) and solid lines represent model used

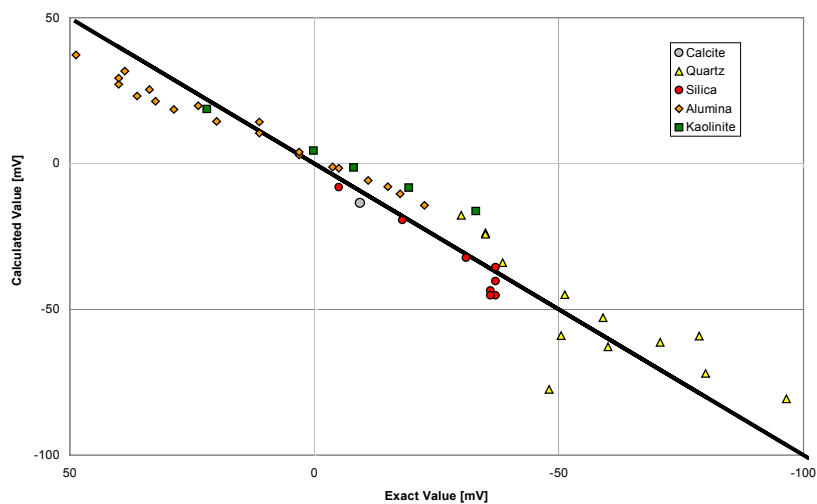


Fig. 14 Cross-plot of calculated vs exact zeta potential values at different temperature and materials

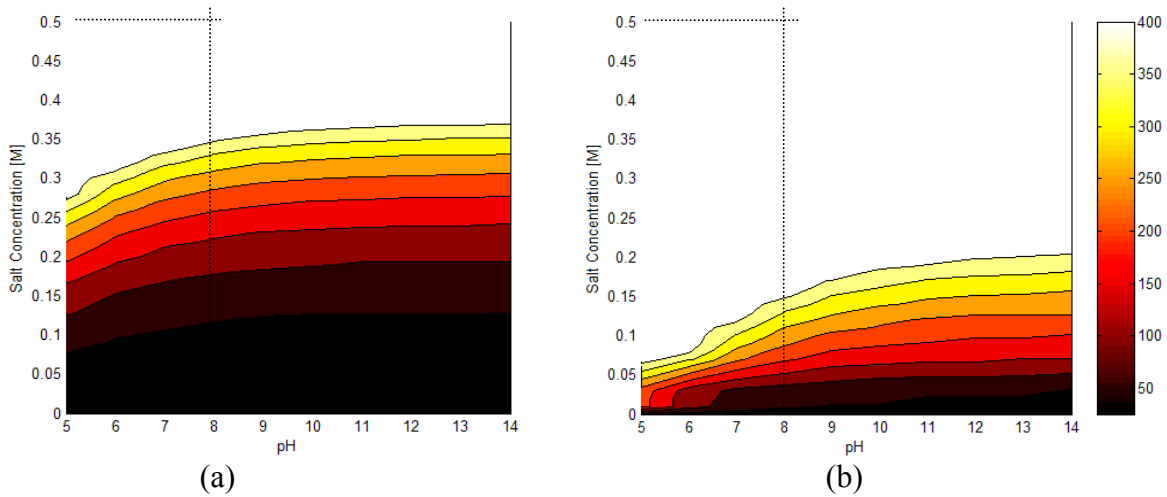


Fig.15 Detachment temperature obtained in sphere-plate model for (a) silica-silica and, (b) silica-kaolinite systems, respectively. Shading is in degree Celsius ( $^{\circ}\text{C}$ )

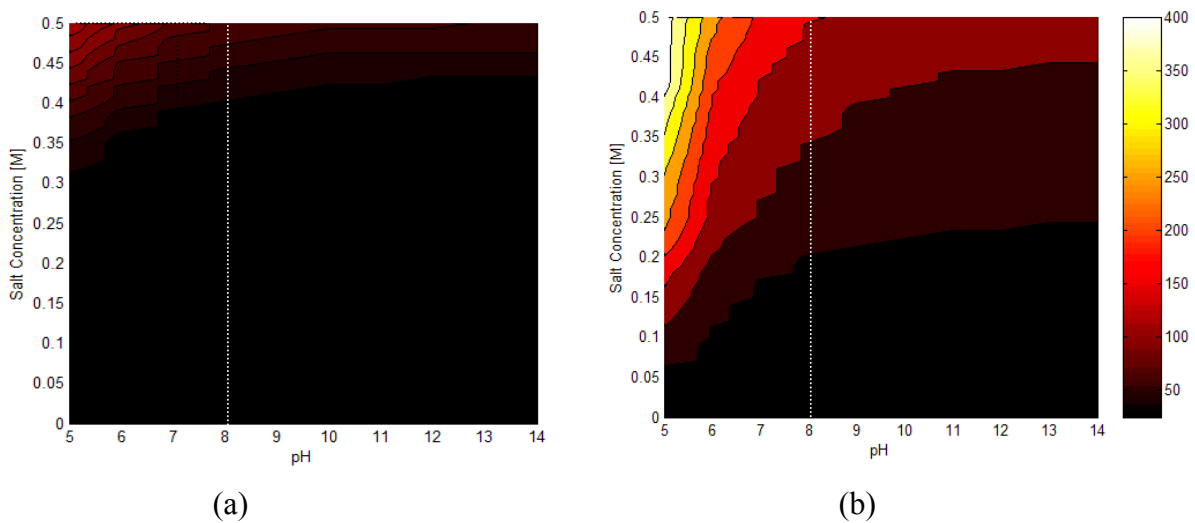


Fig.16 Detachment temperature obtained in cylinder-plate model for (a) silica-silica and, (b) silica-kaolinite systems, respectively. Shading is in degree Celsius ( $^{\circ}\text{C}$ )

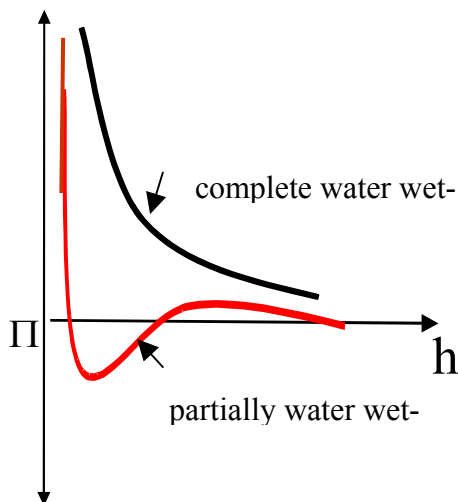


Fig.17 Disjoining pressure isotherm for complete and partially water-wet systems

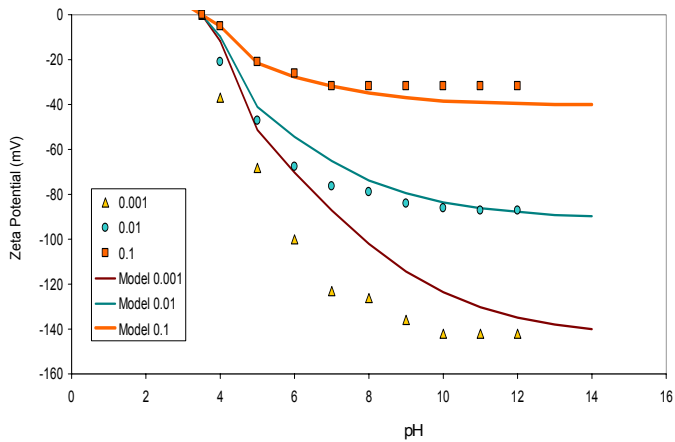


Fig. 18: Zeta potential for Moutray oil at different salt concentrations:  
 symbols: exp. data (Buckley et al, 1989)  
 lines: model used in calculations

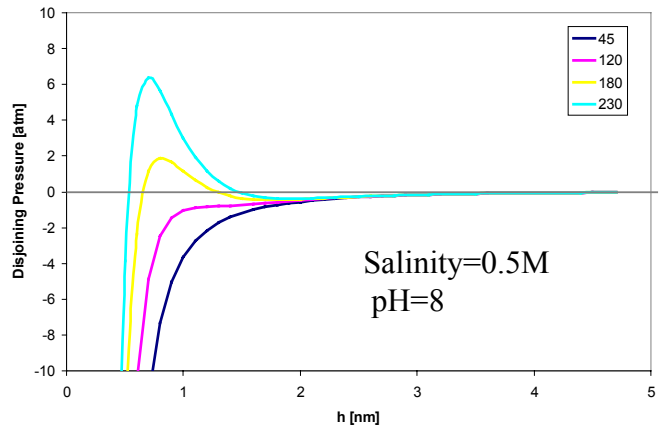


Fig. 19: Disjoining pressures for silica/water/Moutray oil at different temperatures

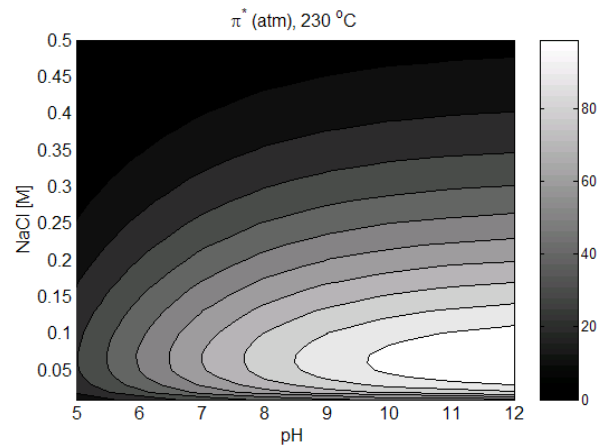
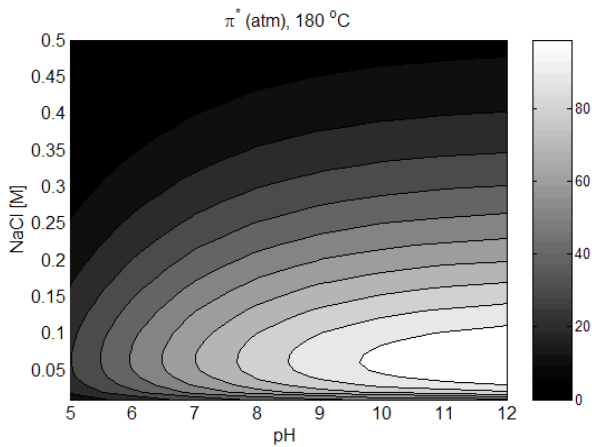
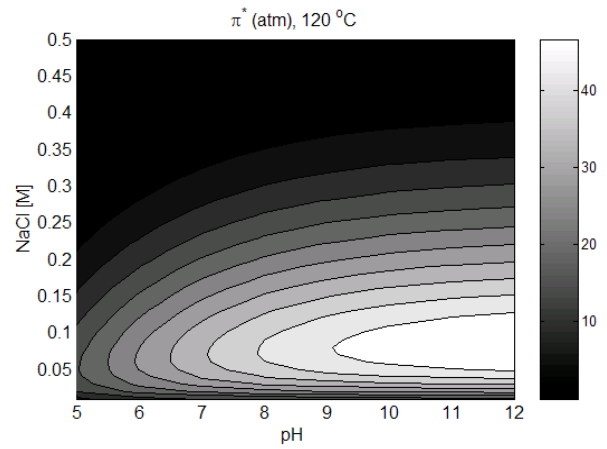
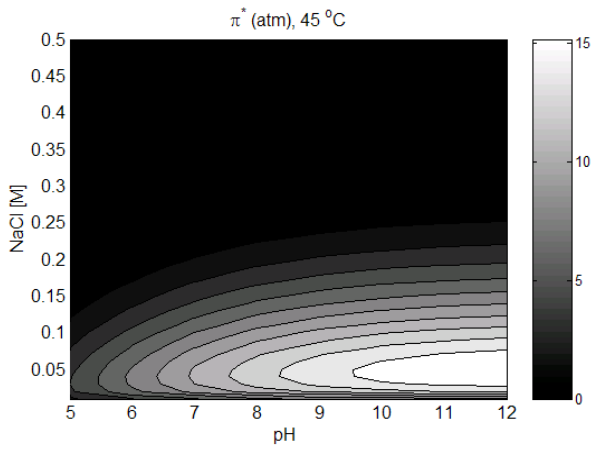


Fig. 20: Critical disjoining pressure isomap (Kpa) for silica/water/Moutray oil at four experimental temperatures (shading is in atm).